Magnetic Materials Hot Paper

International Edition: DOI: 10.1002/anie.201604647
German Edition: DOI: 10.1002/ange.201604647

Multimetal-Substituted Epsilon-Iron Oxide ε-$Ga_{0.31}Ti_{0.05}Co_{0.05}Fe_{1.59}O_3$ for Next-Generation Magnetic Recording Tape in the Big-Data Era

Shin-ichi Ohkoshi, Asuka Namai, Marie Yoshikiyo, Kenta Imoto, Kazunori Tamazaki, Koji Matsuno, Osamu Inoue, Tsutomu Ide, Kenji Masada, Masahiro Goto, Takashi Goto, Takayuki Yoshida, and Tatsuro Miyazaki*

Abstract: *From the viewpoints of large capacity, long-term guarantee, and low cost, interest in magnetic recording tapes has undergone a revival as an archive storage media for big data. Herein, we prepared a new series of metal-substituted ε-Fe_2O_3, ε-$Ga^{III}_{0.31}Ti^{IV}_{0.05}Co^{II}_{0.05}Fe^{III}_{1.59}O_3$, nanoparticles with an average size of 18 nm. Ga, Ti, and Co cations tune the magnetic properties of ε-Fe_2O_3 to the specifications demanded for a magnetic recording tape. The coercive field was tuned to 2.7 kOe by introduction of single-ion anisotropy on Co^{II} ($S = 3/2$) along the c-axis. The saturation magnetization was increased by 44% with Ga^{III} ($S = 0$) and Ti^{IV} ($S = 0$) substitution through the enhancement of positive sublattice magnetizations. The magnetic tape media was fabricated using an actual production line and showed a very sharp signal response and a remarkably high signal-to-noise ratio compared to the currently used magnetic tape.*

To achieve high-density magnetic recording media, the magnetic particles must be downsized.[1–5] Magnetic recording tapes are expected to play an important role in the big-data era due to their long-term guarantee and low cost.[6–8] Magnetic recording tapes are now used for data archiving in insurance companies, banks, broadcasters, and web services. In the current market, the spindle-shaped cobalt–iron alloy nanoparticle is the main magnetic material in recording tapes, but downsizing this alloy is difficult due to its pyrophoric character and the disappearance of its magnetic ordering. Recently, barium ferrite has also started to be used. In 2004, a single phase of ε-Fe_2O_3 was first prepared by combining the reverse-micelle and sol–gel methods. This material exhibits a large coercive field (H_c) over 20 kOe at room temperature.[9] Since then, various studies have been reported.[10–22] In such a high H_c ferrite magnet, the particle size can be downsized because the superparamagnetic limitation size (d_s) is very small (i.e., d_s is 7.5 nm).[22] To adjust the performance of the magnetic material for magnetic recording systems, the H_c value must be tuned to 3 kOe.

Herein, we synthesized multimetal-substituted ε-Fe_2O_3 containing Ga^{3+}, Ti^{4+}, and Co^{2+} ions, ε-$Ga^{III}_{0.31}Ti^{IV}_{0.05}Co^{II}_{0.05}Fe^{III}_{1.59}O_3$. The sample is composed of spherical nanoparticles with an average particle size of 18 nm, and its H_c value was tuned to 2.9 kOe, which is suitable for a high-density magnetic memory. Using this material, we manufactured a practical magnetic recording tape, and demonstrated its performance as a next-generation magnetic recording material.

The target material ε-$Ga_{0.31}Ti_{0.05}Co_{0.05}Fe_{1.59}O_3$ was synthesized using the sol–gel method, where an aqueous solution of $Fe(NO_3)_3$, $Ga(NO_3)_3$, $Co(NO_3)_2$, and $Ti(SO_4)_2$ was mixed with NH_3 aqueous solution to obtain metal hydroxide nanoparticles. Then the metal hydroxide nanoparticles were covered with SiO_2 matrix, and subsequently sintered at 1075 °C for 4 h in air. The SiO_2 matrices were etched by a NaOH solution, and the sample was obtained as brown powder. The formula was determined to be $Ga_{0.31}Ti_{0.05}Co_{0.05}Fe_{1.59}O_3$ according to the X-ray fluorescence (XRF) measurement.

The X-ray powder diffraction (XRPD) measurement shows that $Ga_{0.31}Ti_{0.05}Co_{0.05}Fe_{1.59}O_3$ has an isomorphic crystal structure with ε-Fe_2O_3. From the Rietveld analysis, the crystal structure is refined with an orthorhombic structure in the $Pna2_1$ space group with lattice constants of $a = 5.0928(2)$ Å, $b = 8.7775(4)$ Å, $c = 9.4484(4)$ Å, and $V = 422.36(3)$ Å^3 (Figure 1). The crystal structure has four non-equivalent Fe sites (A–D; i.e., the coordination geometries of the A and B sites are distorted octahedral, the C site is regular octahedral, and the D site is tetrahedral). Ga^{3+}, Ti^{4+}, and Co^{2+} ions predominantly occupy the D sites followed by the C sites; Ga^{3+} occupies 48% of the D sites and 14% of the C sites, Ti^{4+} occupies 10% of the D sites, and Co^{2+} occupies 10% of the D sites. The transmission electron microscopy (TEM) images show that the obtained sample is composed of spherical nanoparticles with a particle size of 18.3 ± 8.8 nm (Figure 1b, inset).

The magnetization versus magnetic field curve shows a magnetization value of 23.4 emu g^{-1} at 7 tesla (Figure 2), while that of the original ε-Fe_2O_3 is 16.2 emu g^{-1}, thus there is a 44% increase upon metal substitution. This magnetization increase can be explained by the reduction in the sublattice magnetization at the D sites due to the substitution of the Fe^{3+} ions ($S = 5/2$) as 48%, 10%, and 10% are replaced by Ga^{3+} ($S = 0$), Ti^{4+} ($S = 0$), and Co^{2+} ($S = 3/2$), respectively. The magnetism of ε-Fe_2O_3 can be understood by collinear ferrimagnetism with a positive sublattice magnetization at

[*] Prof. S. Ohkoshi, Dr. A. Namai, M. Yoshikiyo, Dr. K. Imoto
Department of Chemistry, School of Science
The University of Tokyo
7-3-1 Hongo, Bunkyo-ku, Tokyo 113-0033 (Japan)
E-mail: ohkoshi@chem.s.u-tokyo.ac.jp
K. Tamazaki, K. Matsuno, O. Inoue, T. Ide
TDK Corporation
2-15-7 Higashi-owada, Ichikawa, Chiba 272–8558 (Japan)
K. Masada, M. Goto, T. Goto, T. Yoshida, T. Miyazaki
Dowa Electronics Materials. Co.,Ltd.
1-3-1 Kaigandori, Minami-ku, Okayama 702-8506 (Japan)

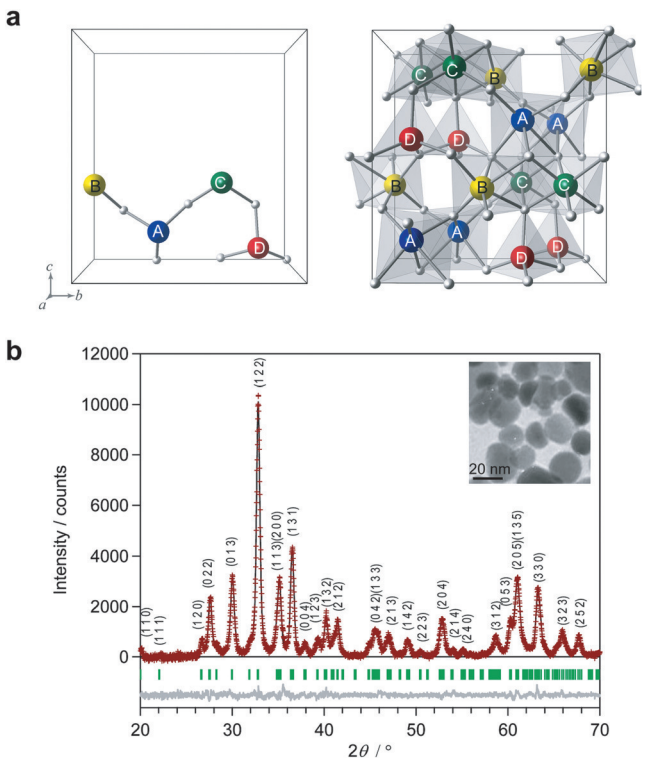

Figure 1. a) Asymmetric unit (left) and unit cell (right) of the ε-$Ga^{III}_{0.31}Ti^{IV}_{0.05}Co^{II}_{0.05}Fe^{III}_{1.59}O_3$ crystal structure shown from the *a*-axis direction. b) XRPD pattern and Rietveld analysis. Observed pattern (red crosses), calculated pattern (black line), and their difference (gray line). Green bars represent the calculated positions of the Bragg reflections of the ε-phase (orthorhombic, $Pna2_1$). Inset: TEM image.

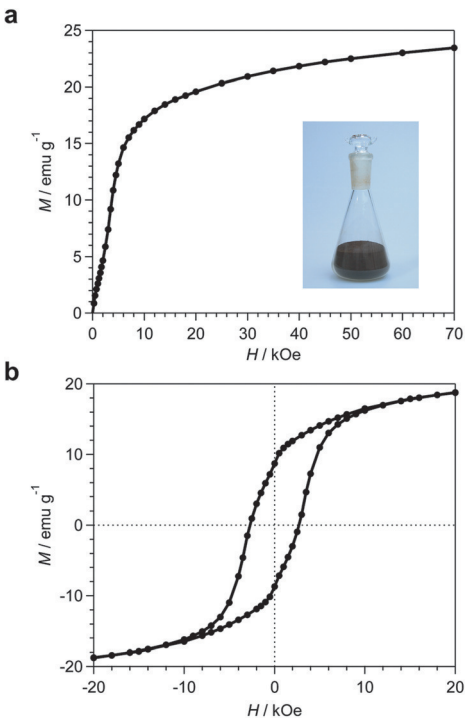

Figure 2. a) Initial magnetization curve and b) magnetic hysteresis loop of ε-$Ga_{0.31}Ti_{0.05}Co_{0.05}Fe_{1.59}O_3$ measured at 300 K. Inset of (a) is a picture of the powder sample.

the B and C sites (M_B, $M_C > 0$) and a negative sublattice magnetization at the A and D sites (M_A, $M_D < 0$) (Figure 3a).[18] Therefore, the reduction of the negative sublattice magnetization at the D sites by metal substitution should contribute to the increased total magnetization (Figure 3b).

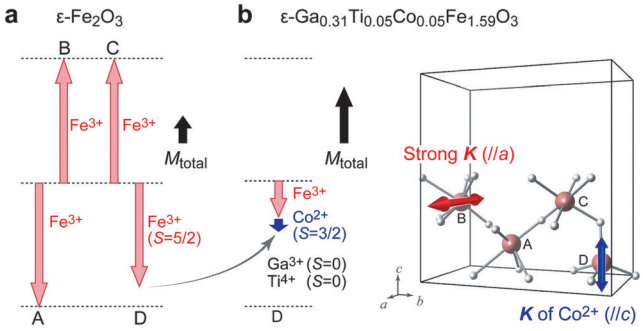

Figure 3. Magnetic structure of ε-Fe_2O_3 (a) and ε-$Ga_{0.31}Ti_{0.05}Co_{0.05}Fe_{1.59}O_3$ (b, left). Red and blue arrows denote the sublattice magnetizations of Fe^{3+} and Co^{2+}, respectively. Upward (downward) arrows denote the positive (negative) sublattice magnetization. Black arrows show the total magnetization. Right part of (b) shows the asymmetric unit in the unit cell denoting the direction of the single-ion anisotropies (*K*, red and blue arrows) for Fe^{3+} at the B site along *a*-axis and Co^{2+} at the D site along *c*-axis.

The magnetic hysteresis loop shows that the H_c value can be tuned below 3 kOe, $H_c = 2.69$ kOe, which is one order smaller than the H_c value of the original ε-Fe_2O_3. This reduction in the H_c value can be explained by the compensation of single-ion anisotropies of Fe^{3+} and the additional Co^{2+}. In the case of ε-Fe_2O_3, the first-principles calculation indicates that the large magnetic anisotropy of ε-Fe_2O_3 along the *a*-axis at room temperature is due to the orbital angular momentum of Fe^{3+} at the B site, which originates from the hybridization between Fe^{3+} ion and O^{2-} ion (Figure 3b).[15] In ε-$Ga_{0.31}Ti_{0.05}Co_{0.05}Fe_{1.59}O_3$, the magnetic anisotropy of the Co^{2+} ion at the D site is considered to be directed along the *c*-axis. Hence, the magnetic anisotropy of Fe^{3+} ion at the B site along the *a*-axis is compensated by that of Co^{2+} ion, resulting in the tuning of H_c below 3 kOe.

One of the requirements of a magnetic recording tape is an H_c value of approximately 3 kOe. Since the H_c value of ε-$Ga_{0.31}Ti_{0.05}Co_{0.05}Fe_{1.59}O_3$ is suitable for magnetic recordings, we synthesized a large amount of this sample (5 kg), and manufactured a trial magnetic tape in an actual factory. The dispersion solution of ε-$Ga_{0.31}Ti_{0.05}Co_{0.05}Fe_{1.59}O_3$ in a resin was coated onto a non-magnetic layer film under an external magnetic field of 7 kOe (Figure 4a; see Experimental section for details). The layered structure of the ε-$Ga_{0.31}Ti_{0.05}Co_{0.05}Fe_{1.59}O_3$ magnetic tape is schematically illustrated in Figure 4b, and the cross-section scanning electron microscopy (SEM) image of the manufactured magnetic tape is shown in Figure 4c. The magnetic layer is 110 ± 5 nm thick and the surface roughness of the magnetic layer is a very low value of 2.7 nm. The magnetic measurement shows that the nanoparticles are crystallographically oriented through the applied magnetic field during the tape preparation. The

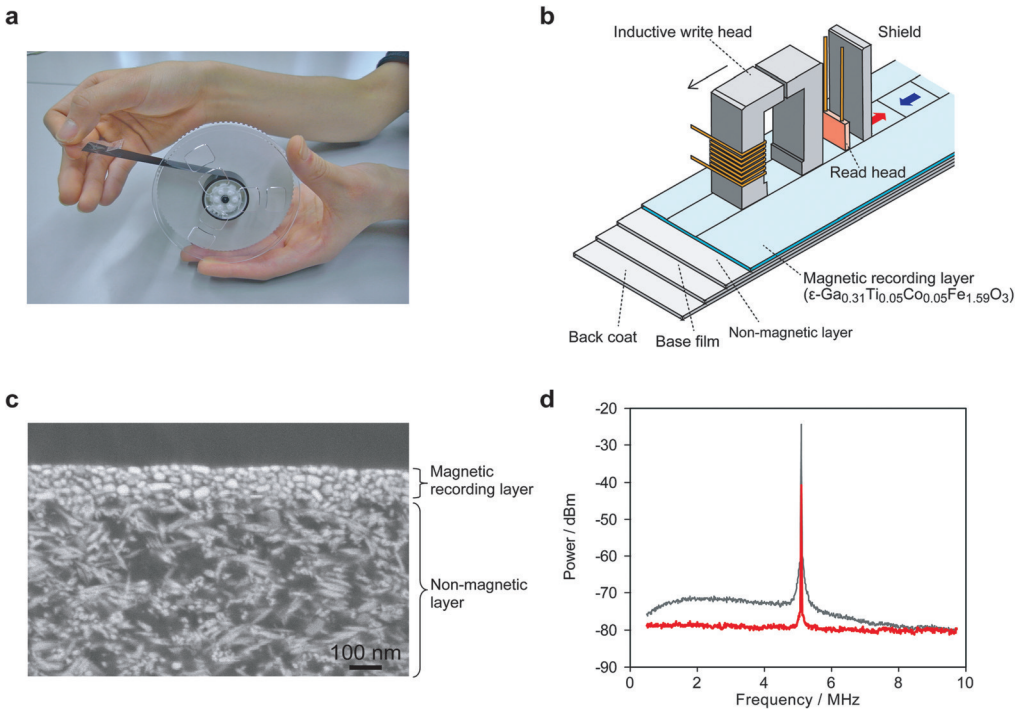

Figure 4. a) Photograph of the manufactured magnetic recording tape composed of ε-$Ga_{0.31}Ti_{0.05}Co_{0.05}Fe_{1.59}O_3$. b) Schematic illustration of the LTO-3 AMR head composed of an inductive write head, a read head, and a shield. c) Cross-section SEM image of the manufactured magnetic tape. d) Power spectrum of the signal of the ε-$Ga_{0.31}Ti_{0.05}Co_{0.05}Fe_{1.59}O_3$ tape (red line) and cobalt–iron alloy tape (gray line) measured with the LTO-3 AMR head.

squareness ratio of the magnetic hysteresis loop, which is defined as the residual magnetic flux density over maximum magnetic flux density, is 0.68, and the H_c value is 2.91 kOe in the longitudinal direction of the magnetic tape.

The performance of the magnetic recording tape was evaluated using a 3rd-generation linear tape-open (LTO-3) anisotropic magnetoresistive (AMR) head (Figure 4b). The recording performance of the ε-$Ga_{0.31}Ti_{0.05}Co_{0.05}Fe_{1.59}O_3$ magnetic recording tape was investigated using a spectrum analyzer, and the results were compared to those of a cobalt–iron metal alloy (MP1, DOWA Electronics Materials) magnetic tape. As shown in Figure 4d, the ε-$Ga_{0.31}Ti_{0.05}Co_{0.05}Fe_{1.59}O_3$ tape gives a very sharp signal peak. The foot of the signal peak is remarkably narrower than that of the MP1 magnetic tape, and the baseline is perfectly flat. These features indicate that the ε-$Ga_{0.31}Ti_{0.05}Co_{0.05}Fe_{1.59}O_3$ magnetic tape has a high signal-to-noise ratio (S/N). Such a remarkably high S/N performance indicates that the present magnetic material has potential in future magnetic-tape recording applications.

In summary, we prepared a new series of metal-substituted ε-Fe_2O_3 nanoparticles, ε-$Ga^{III}_{0.31}Ti^{IV}_{0.05}Co^{II}_{0.05}Fe^{III}_{1.59}O_3$, with an average size of 18 nm. Ga^{3+}, Ti^{4+}, and Co^{2+} cations tune the magnetic properties of ε-Fe_2O_3 to the specifications demanded for a magnetic recording tape, and we demonstrated that it is useful for the magnetic recording storage system. This series of materials should be applicable for data storage in the big-data era as it should realize high-density economical and long-guarantee magnetic recording media.

Experimental Section

Material characterization and magnetic measurement: Elemental analyses of the prepared samples were performed using an XRF spectrometer, Rigaku ZSX Primus II. Calcd (%): Ga 13.4, Ti 1.4, Co 1.7, and Fe, 54.2. Found: Ga 13.1, Ti 1.4, Co 1.7, and Fe, 53.4. The TEM measurements were conducted using a JEOL JEM-2000EXII and 100CX-Mark II, while the X-ray powder diffraction (XRPD) measurements were conducted by a Rigaku Ultima IV with Cu Kα radiation ($\lambda = 1.5418$ Å). Rietveld analysis was performed by the RIETAN-FP program. The magnetic properties were measured using a superconducting quantum interference device (SQUID) magnetometer (Quantum Design, MPMS 7) and a Quantum Design 6000 physical property measurement system (PPMS).

Preparation of the magnetic tape: ε-$Ga_{0.31}Ti_{0.05}Co_{0.05}Fe_{1.59}O_3$ powder sample was mixed into a resin solution composed of polyurethane and polyvinylchloride dissolved in methylethylketone, toluene, and cyclohexane. The dispersion was coated on a non-magnetic layer on a base film. The non-magnetic layer was composed of spindle-shaped hematite, carbon, and an Al_2O_3. PEN film of Teijin DuPont was used for the base film. The ε-$Ga_{0.31}Ti_{0.05}Co_{0.05}Fe_{1.59}O_3$ particles were oriented in the resin under an external magnetic field of 7 kOe along the longitudinal direction of the tape. TEM and SEM images of the magnetic recording tapes were acquired using JEOL 3010 and HITACHI S4700, respectively.

Acknowledgements

The research was supported in part by JSPS Grant-in-Aid for Specially Promoted Research (Grant Number 15H05697), JSPS Grant-in-Aid for Young Scientists (B), ACCEL-FS project of JST, and DOWA Technofund. We also recognize

the Cryogenic Research Center, the University of Tokyo, APSA, and Nanotechnology Platform, which are supported by MEXT.

Keywords: epsilon-iron oxide · hard magnetic ferrite · iron · magnetic properties · magnetic recording tape · nanoparticles

How to cite: *Angew. Chem. Int. Ed.* **2016**, *55*, 11403–11406
Angew. Chem. **2016**, *128*, 11575–11578

[1] M. L. Plumer, J. van Ek, D. Weller, *The Physics of Ultra-High Density Magnetic Recording*, Springer, Berlin, **2001**.
[2] W. A. Challener, C. Peng, A. V. Itagi, D. Karns, W. Peng, Y. Peng, X. M. Yang, X. Zhu, N. J. Gokemeijer, Y.-T. Hsia, G. Ju, R. E. Rottmayer, M. A. Seigler, E. C. Gage, *Nat. Photonics* **2009**, *3*, 220.
[3] T. Hayashi, S. Hirono, M. Tomita, S. Umemura, *Nature* **1996**, *381*, 772.
[4] I. Tudosa, C. Stamm, A. B. Kashuba, F. King, H. C. Siegmann, J. Stöhr, G. Ju, B. Lu, D. Weller, *Nature* **2004**, *428*, 831.
[5] D. Alloyeau, C. Ricolleau, C. Mottet, T. Oikawa, C. Langlois, Y. Le Bouar, N. Braidy, A. Loiseau, *Nat. Mater.* **2009**, *8*, 940.
[6] G. Cherubini, C. C. Chung, W. C. Messner, S. O. R. Moheimani, *IEEE Trans. Contr. Syst. Technol.* **2012**, *20*, 296.
[7] H. Nishio, H. Yamamoto, *IEEE Trans. Magn.* **2010**, *46*, 3747.
[8] R. E. Fontana, Jr., G. M. Decad, S. R. Hetzler, *J. Appl. Phys.* **2015**, *117*, 17E301.
[9] J. Jin, S. Ohkoshi, K. Hashimoto, *Adv. Mater.* **2004**, *16*, 48.
[10] E. Tronc, C. Chanéac, J. P. Jolivet, J. M. Grenèche, *J. Appl. Phys.* **2005**, *98*, 053901.
[11] S. Ohkoshi, S. Kuroki, S. Sakurai, K. Matsumoto, K. Sato, S. Sasaki, *Angew. Chem. Int. Ed.* **2007**, *46*, 8392; *Angew. Chem.* **2007**, *119*, 8544.
[12] Y.-C. Tseng, N. M. Souza-Neto, D. Haskel, M. Gich, C. Fontera, A. Roig, M. van Veenendaal, J. Nogués, et al., *Phys. Rev. B* **2009**, *79*, 094404.
[13] A. Namai, S. Sakurai, T. Suemoto, M. Nakajima, K. Matsumoto, M. Goto, S. Sasaki, S. Ohkoshi, *J. Am. Chem. Soc.* **2009**, *131*, 1170.
[14] J. Tuček, R. Zbořil, A. Namai, S. Ohkoshi, *Chem. Mater.* **2010**, *22*, 6483.
[15] A. Namai, M. Yoshikiyo, K. Yamada, S. Sakurai, T. Goto, T. Yoshida, T. Miyazaki, M. Nakajima, T. Suemoto, H. Tokoro, S. Ohkoshi, *Nat. Commun.* **2012**, *3*, 1035.
[16] M. Gich, I. Fina, A. Morelli, F. Sánchez, M. Alexe, J. Gàzquez, J. Fontcuberta, A. Roig, *Adv. Mater.* **2014**, *26*, 4645.
[17] P. Brázda, E. Večerníková, E. Pližingrová, A. Lančok, D. Nižňansky, *J. Therm. Anal. Calorim.* **2014**, *117*, 85.
[18] S. Ohkoshi, H. Tokoro, *Bull. Chem. Soc. Jpn.* **2013**, *86*, 897.
[19] D. A. Balaev, I. S. Poperechny, A. A. Krasikov, K. A. Shaikhutdinov, A. A. Dubrovskiy, S. I. Popkov, A. D. Balaev, S. S. Yakushkin, G. A. Bukhtiyarova, O. N. Martyanov, Yu. L. Raikher, *J. Appl. Phys.* **2015**, *117*, 063908.
[20] J. Kohout, P. Brázda, K. Závěta, D. Kubániová, T. Kmječ, L. Kubíčková, M. Klementová, E. Šantavá, A. Lančok, *J. Appl. Phys.* **2015**, *117*, 17D505.
[21] A. A. Dubrovskiy, D. A. Balaev, K. A. Shaykhutdinov, O. A. Bayukov, O. N. Pletnev, S. S. Yakushkin, G. A. Bukhtiyarova, O. N. Martyanov, *J. Appl. Phys.* **2015**, *118*, 213901.
[22] S. Ohkoshi, A. Namai, K. Imoto, M. Yoshikiyo, W. Tarora, K. Nakagawa, M. Komine, Y. Miyamoto, T. Nasu, S. Oka, H. Tokoro, *Sci. Rep.* **2015**, *5*, 14414.

Received: May 12, 2016
Published online: August 24, 2016

